INL/EXT-16-40050

Light Water Reactor Sustainability Program

Probabilistic Fracture Mechanics of Reactor Pressure Vessels with Populations of Flaws

Benjamin W. Spencer
Marie Backman
Paul T. Williams
William M. Hoffman
Andrea Alfonsi
Terry L. Dickson
B. Richard Bass
Hilda B. Klasky

September 2016

DOE Office of Nuclear Energy

INL/EXT-16-40050

Light Water Reactor Sustainability Program

Probabilistic Fracture Mechanics of Reactor Pressure Vessels with Populations of Flaws

Benjamin W. Spencer – INL
Marie Backman – University of Tennessee
Paul T. Williams – ORNL
William M. Hoffman – INL
Andrea Alfonsi – INL
Terry L. Dickson – ORNL
B. Richard Bass – ORNL
Hilda B. Klasky – ORNL

September 2016

Idaho National Laboratory
Idaho Falls, Idaho 83415

http://www.inl.gov/lwrs

Prepared for the
U.S. Department of Energy
Office of Nuclear Energy
Under DOE Idaho Operations Office
Contract DE-AC07-05ID14517

ABSTRACT

This report documents recent progress in developing a tool that uses the Grizzly and RAVEN codes to perform probabilistic fracture mechanics analyses of reactor pressure vessels in light water reactor nuclear power plants. The Grizzly code is being developed with the goal of creating a general tool that can be applied to study a variety of degradation mechanisms in nuclear power plant components. Because of the central role of the reactor pressure vessel (RPV) in a nuclear power plant, particular emphasis is being placed on developing capabilities to model fracture in embrittled RPVs to aid in the process surrounding decision making relating to life extension of existing plants.

A typical RPV contains a large population of pre-existing flaws introduced during the manufacturing process. The use of probabilistic techniques is necessary to assess the likelihood of crack initiation at one or more of these flaws during a transient event. This report documents development and initial testing of a capability to perform probabilistic fracture mechanics of large populations of flaws in RPVs using reduced order models to compute fracture parameters. The work documented here builds on prior efforts to perform probabilistic analyses of a single flaw with uncertain parameters, as well as earlier work to develop deterministic capabilities to model the thermo-mechanical response of the RPV under transient events, and compute fracture mechanics parameters at locations of pre-defined flaws.

The capabilities developed as part of this work provide a foundation for future work, which will develop a platform that provides the flexibility needed to consider scenarios that cannot be addressed with the tools used in current practice.

CONTENTS

FIGURES

ACRONYMS

CPI	Conditional Probability of Initiation
INL	Idaho National Laboratory
LWR	Light Water Reactor
LWRS	Light Water Reactor Sustainability
ORNL	Oak Ridge National Laboratory
PFM	Probabilistic Fracture Mechanics
PTS	Pressurized Thermal Shock
PWR	Pressurized Water Reactor
RISMC	Risk-Informed Safety Margin Characterization
ROM	Reduced Order Model
RPV	Reactor Pressure Vessel
RSM	Response Surface Methodology
SIFIC	Stress Intensity Factor Influence Coefficient

1 Introduction

The Grizzly code is one of the suite of tools being developed under the Risk-Informed Safety Margin Characterization (RISMC) Pathway in the U.S. Department of Energy's Light Water Reactor Sustainability (LWRS) program. Grizzly is a tool for simulating aging mechanisms and predicting the capacity of aged systems, structures, and components in existing light water reactor (LWR) nuclear power plants. The goal of Grizzly is to enable the use of physics-based models to improve confidence in predictions of the effects of aging. This will permit better-informed decision making as long term operation of plants is considered.

The initial focus of Grizzly development has been on aging mechanisms and capacity of reactor pressure vessels (RPVs). The primary concern in considering the integrity of an RPV during a transient event is that fracture may initiate at the location of a pre-existing flaw introduced during the manufacturing process. Over time, exposure to irradiation and elevated temperature embrittles the material, making it more susceptible to fracture. Efforts are being made both to model the microstructure and engineering properties of RPV steel, as well as to develop a modern, flexible tool for engineering analysis of RPVs subjected to transients.

Much of the work to-date on the engineering analysis tools in Grizzly has been focused on developing deterministic analysis capabilities. Typical RPVs contain large populations of flaws with uncertain characteristics, so probabilistic techniques lend themselves well to providing better understanding of the risks associated with RPV fracture. A recent report [1] documents initial efforts to develop a probabilistic fracture mechanics (PFM) capability using a combination of Grizzly and RAVEN, the RISMC code for probabilistic analysis. That prior work resulted in a capability to compute the conditional probability of initiation (CPI) of fracture at a single flaw of a given geometry, considering uncertainty in the composition of the alloying elements in the RPV steel.

The work documented here greatly expands on that prior work. The tools previously developed have been extended to allow for the consideration of large and uncertain populations of flaws in RPVs, to enable a computation of the overall probability of initiation of a fracture at any of the flaws present in an RPV during a transient event. Because of the large numbers of flaws that must be considered, the models to compute the stress intensity factors at flaws must be able to be evaluated with minimal computational expense. To that end, capabilities to compute these fracture mechanics parameters using reduced order models (ROMs) have been implemented in this tool.

The FAVOR (Fracture Analysis of Vessels - Oak Ridge) [2, 3] code is widely used and accepted as a tool for PFM analysis of RPVs. The present work has been done in collaboration with the FAVOR team at Oak Ridge National Laboratory (ORNL), and replicates many of the capabilities of FAVOR in the RISMC toolset. Initial benchmarking of some aspects of this code against FAVOR have been performed. The longer-term goal of this work is not to simply replicate FAVOR's capabilities, but to develop a more flexible analysis tool that can be easily extended to consider effects that are beyond the scope of FAVOR's capabilities.

This report is organized as follows: Section 2 describes the sampling algorithm used for PFM of flaw populations, with details on how this is implemented in Grizzly/RAVEN. Section 3 describes the results of initial benchmarking of this capability. Section 4 provides a summary of this work, including ongoing and planned future work in this area.

2 Algorithm Structure

The procedure for computing the probability of failure of an RPV with a population of flaws involves a number of steps, which must be appropriately combined together. A widely accepted Monte Carlo-based process for sampling random populations of flaws and embrittlement-related variables and evaluating the probability of failure of an RPV has been developed over multiple decades in the FAVOR code. The work documented here is an effort to replicate this process using codes in the RISMC toolkit – Grizzly and RAVEN. While the current work essentially replicates capabilities that already exist in FAVOR, it also provides a foundation for adding much more flexibility in the way these calculations are performed.

This section first provides an overview of the overall structure of the sampling algorithm, and then provides details on the individual components of that algorithm and their implementation in Grizzly/RAVEN.

2.1 Overall Structure of Sampling Algorithm

2.1.1 FAVOR methodology

Because the methodology used by FAVOR served as a template for the current effort, the overall algorithm will begin with a discussion of the flow of the algorithm used by FAVOR. The FAVOR code consists of three separate applications that together provide a PFM capability for RPVs. These three codes are FAVLOAD, which computes the thermomechanical response of the RPV, FAVPFM, which performs probabilistic analysis of populations of flaws, and FAVPOST, which performs postprocessing on the results. These three codes are run in that sequence. It is assumed that there is no two-way feedback between the global, far-field response of the RPV and the flaws, so the FAVLOAD module is run initially to provide boundary conditions for the PFM analysis.

Figure 1 shows a flowchart of the overall algorithm used by the FAVOR code suite, including the global response, PFM, and postprocessing phases. An important aspect of this algorithm is that the PFM analysis includes a two-level sampling scheme. Monte Carlo sampling is used at two levels. At the outer level, a series of realizations of RPVs are generated. Each RPV realization consists of samples of global variables, steel chemistry parameters that apply globally to the major regions of the RPV, and a random flaw population whose geometric characteristics are defined by probability distributions. A different number of flaws is generated for each RPV realization.

At the inner level, steel chemistry parameters are generated for each of the flaws in an RPV realization. These are local perturbations to the global properties of the major region (plate, weld, fusion zone) in which they are located. Using these chemistry parameters, the conditional probability of initiation (CPI) and conditional probability of failure (CPF) is computed for each flaw. These are the probability of a fracture initiating at that flaw, and the probability that fracture propagating through the vessel, conditional on occurrence of the given transient loading. The first step of this calculation is to characterize the embrittlement of the steel by computing the ductile to brittle transition temperature, RT_{NDT}. For each time step in a given transient, K_I, the mode I stress intensity factor, is computed using closed-form expressions to compute it as a function of the far-field stresses and flaw geometry. A Weibull model is then used to compute the instantaneous conditional probability of initiation (CPI) of a fracture at that flaw. The maximum value of CPI over time is taken as the CPI for a given flaw.

FAVOR provides the ability to evaluate a set of transient events in a single run. When considering multiple transient events, it is important to apply the same flaw population to all of those transients, so the loop over these transients is done within the loop over the flaws in an RPV. The result of this calculation is a vector of CPIs, one for each transient.

Following the computation of CPI, if there is a nonzero CPI, an initiation-growth-arrest model is employed to compute the CPF, which can be less than or equal to the CPI. The current work has focused only

on the computation of CPI, so this model is not described here.

When all flaws in a given RPV realization have been processed, an aggregate CPI for initiation of fracture at any of the flaws in that vessel realization under a given transient is computed as:

$$CPI_{RPV} = 1 - \prod_{i=1}^{nflaw} (1 - CPI_i) \tag{1}$$

Once FAVPFM has completed, FAVPOST combines CPI and CPF values for each realization with sampled values of frequency of occurrence of transients to compute the frequency of crack initiation and the frequency of vessel failure (i.e. failures/operating year).

2.1.2 Grizzly/RAVEN implementation

The goal of the present work was to replicate as closely as possible the PFM methodology used by FAVOR using the Grizzly and RAVEN codes. Figure 2 shows a flowchart of the algorithm as implemented in Grizzly/RAVEN. The large boxes containing sections of the algorithm indicate the code objects that were developed to perform these functions. Not all of the features of FAVOR have been implemented in Grizzly/RAVEN yet. Notably, the current implementation supports evaluation of only a single transient, and does not have the initiation-growth-arrest algorithm necessary to compute CPF. The nodes in the flow chart relating those features are included to indicate how they will fit in this structure, but are cross-hatched to indicate that they have not yet been implemented.

One of the major challenges that had to be addressed in this implementation was that RAVEN does not provide a way to nest sampling loops. Because of this, the structure of the sampling had to be modified, as indicated in Figure 2. The employed sampling strategy flattens out the nested loops into a single loop over all of the flaws in every RPV realization. When each flaw is evaluated, the full set of input and output variables associated with that sample and its calculation are stored. An additional output variable that stores an identifier for the RPV realization that the flaw sample is associated with is stored for each sample. To compute the aggregate CPI for each RPV, an additional postprocessing step is taken in which all of the samples for a given RPV realization are assembled based on the RPV realization identifier, and Equation 1 is applied separately to each grouped set of flaws.

In this algorithm, the sampler simply loops through flaws until it reaches the last flaw in the last RPV realization. The first time a sample is requested, a population of flaws for the first RPV realization is generated and stored. Subsequent samples are taken from this stored flaw population until the last flaw in that set is used, and then a new population of flaws is generated and stored for the next RPV. When the flaws are generated for an RPV, sampling of other variables that are global to an RPV is also performed, and those are stored for use in the computation of random variables for individual flaws in that RPV.

In addition to describing the flow of the algorithm, Figure 2 also indicates the code modules that are used to implement its various components. Prior to the PFM phase of the analysis, Grizzly is used to compute the global thermomechanical response of the RPV. In the current work, this is done using a strip of elements in a 2D axisymmetric model with appropriate boundary conditions to approximate the behavior of an infinite cylinder. This is compatible with the approach used by FAVOR, and prior benchmarking has demonstrated that the two codes produce equivalent results. Grizzly is able to compute this response on a full 2D axisymmetric or 3D model of the RPV as well. This capability will be used in the future in conjunction with the PFM capability described here to evaluate scenarios that require higher dimensionality representations of the RPV.

The RAVEN code is written in the Python language, and is written as an extensible object-oriented framework. Many of the features of the code are implemented using a combination of base classes (to define interfaces to functionality) and derived classes (to implement that functionality for specific cases).

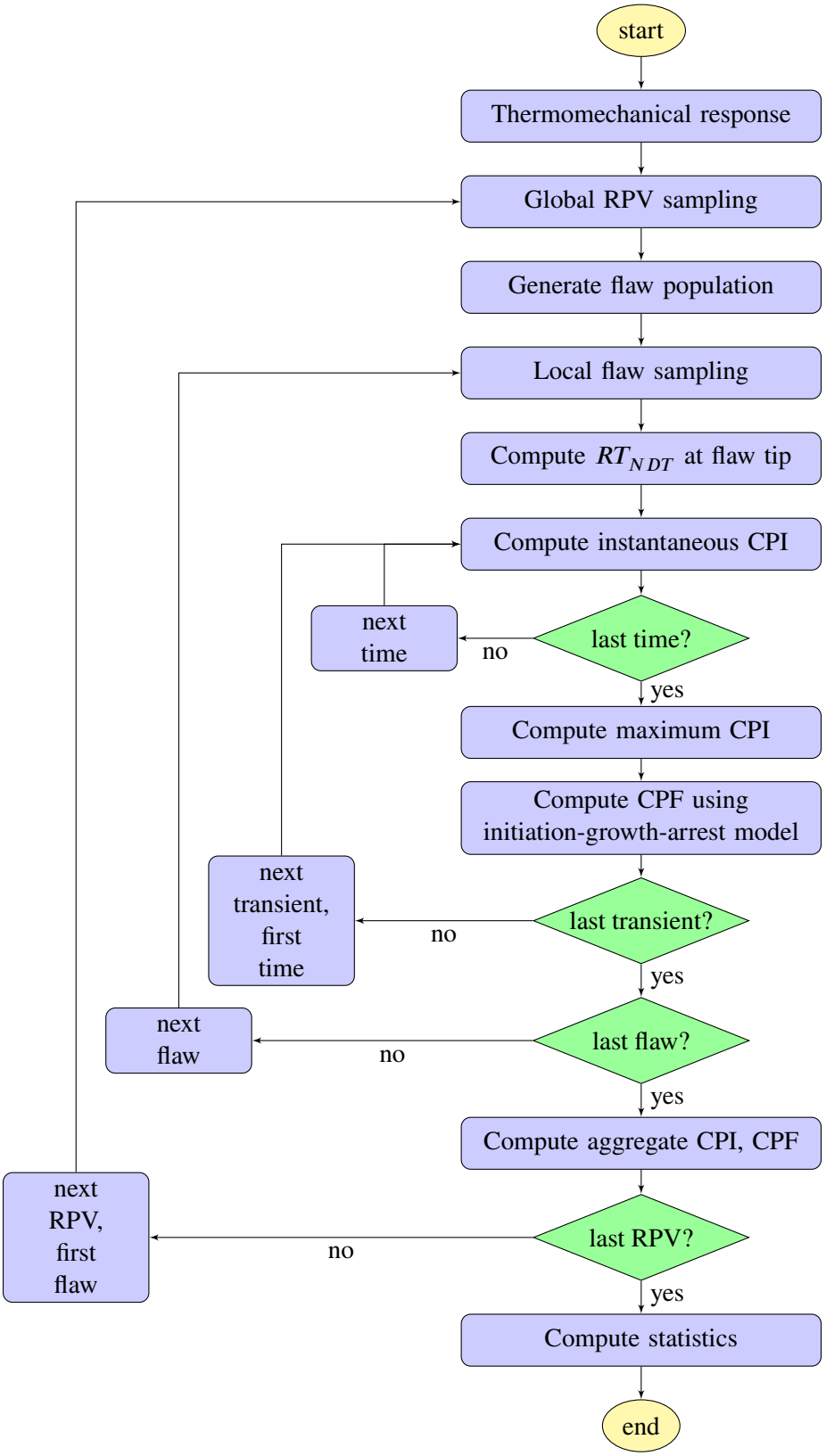

Figure 1: Flowchart of algorithm used by FAVOR for probabilistic fracture mechanics with a flaw population

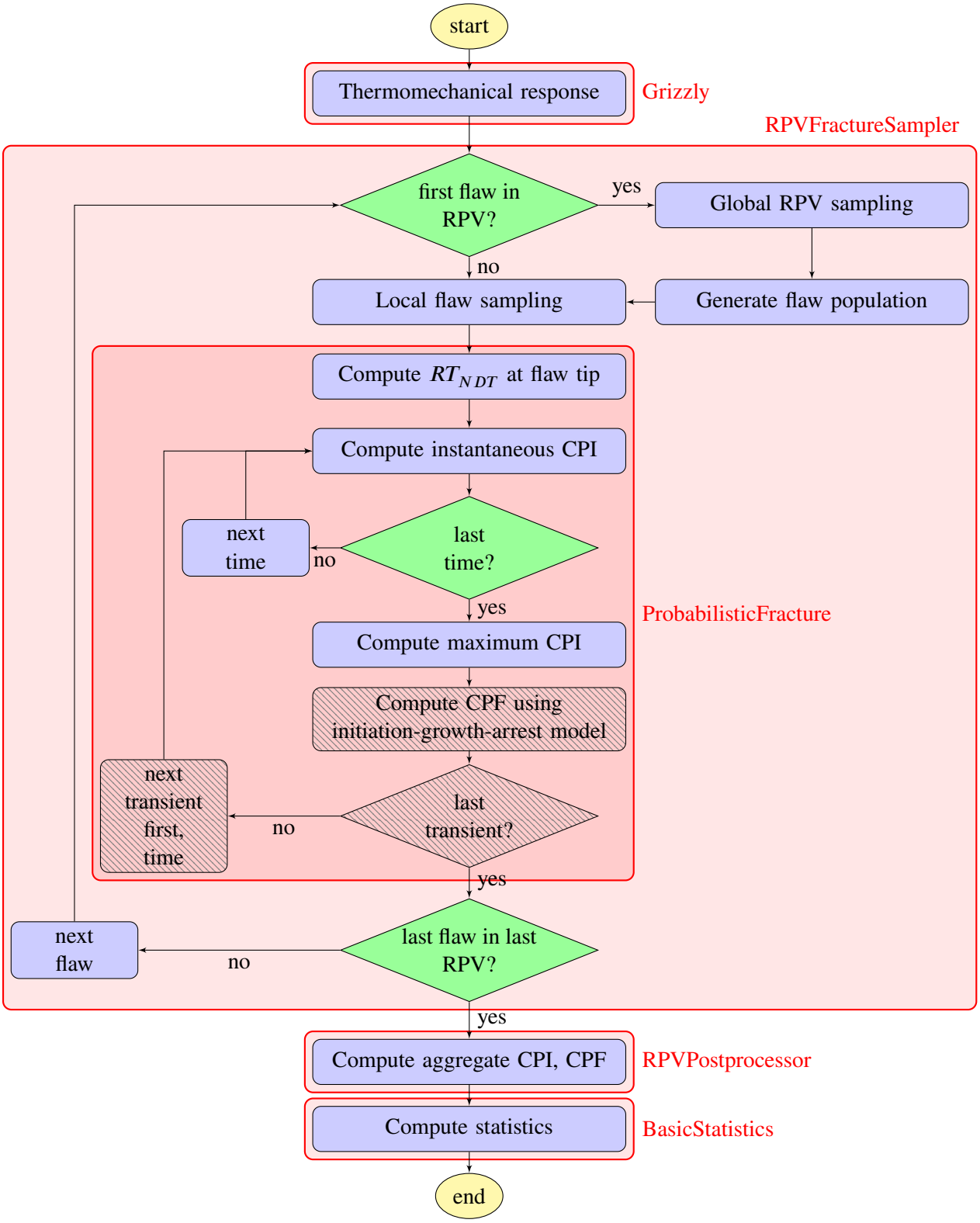

Figure 2: Flowchart of algorithm used by Grizzly/RAVEN for probabilistic fracture mechanics with a flaw population. Cross-hatched nodes represent capabilities that have not yet been implemented.

The capability described here was implemented using three specialized inherited classes that extend the base functionality of RAVEN for the RPV PFM application.

The sampling algorithm is implemented using a Python class called `RPVFractureSampler` that derives from the base `Sampler` class in RAVEN. This class provides all of the functionality needed to generate the flaw samples with all of the associated random variables based on the methodology used by FAVOR. It generates the flaw population for each RPV realization, including geometric characteristics and assignment of flaws to major regions in the vessel and appropriate sampling of steel chemistry variables.

The `RPVFractureSampler` offers flexibility in the ways that flaws can be defined. It can generate the flaw population using sampling based on distributions of flaw geometric characteristics. It alternatively allows for the geometric characteristics of each individual flaw to be read in from a text file containing that data formatted as a comma-separated table. This can be useful for evaluating scenarios where the flaw population is known. Alternatively, PFM analyses can be performed without using `RPVFractureSampler` at all. Any of the other `Sampler` classes in RAVEN can be used as long as the appropriate set of variables defining the flaws is defined. For instance, the `CustomSampler` can be used to read in a comma-separated text table containing the full set of parameters for a set of flaws, including flaw geometry and chemistry parameters. This can be very useful for debugging and benchmarking purposes to compute the CPI for specific flaws with specific parameters.

Most of the specialized classes developed for this capability are maintained in the Grizzly code repository. RAVEN currently provides application programming interfaces (APIs) that allow users to write custom classes that derive from many of the base classes, and the code for these classes can exist in another location than the RAVEN code directory structure. Such support does not currently exist for the `Sampler` class. As a result, the code must currently be implemented in the RAVEN code directory structure. Because this capability is specific for RPV analysis, it cannot be distributed with the rest of the RAVEN code base, so it currently exists in a development version of RAVEN that is not distributed. There are plans to develop an API to permit users to extend the `Sampler` class. This code will be added to the Grizzly code base for distribution with Grizzly at that time.

All calculations needed to compute CPI for a given flaw are done in the `ProbabilisticFracture` module, which is implemented as a RAVEN `ExternalModel`. This code computes the ductile to brittle transition temperature, RT_{NDT} for a specific flaw using the EONY model [4]. It then uses a reduced order model to compute the K_I history of the flaw, as described in detail in Section 2.5. An early version of the `ProbabilisticFracture` module was described in [5]. That initial version required a K_I history as input. For the present work, this module was extended to allow for it to either internally compute K_I histories for embedded and surface-breaking flaws using reduced order models, or read them in from a file.

Finally, the `RPVPostprocessor` module was developed to compute the aggregate CPI for the set of flaws associated with an RPV. This class, which derives from the `Postprocessor` base class in RAVEN, takes the set of inputs and outputs for all flaws, and generates as output a smaller array of aggregate CPIs for each RPV realization.

2.2 Flaw Geometry Sampling

The flaw populations in FAVOR are generated using files that define a set of distributions of flaw density, depth, and aspect ratio. These files are generated using the VFLAW tool developed by Pacific Northwest National Laboratory as part of the NRC's PTS Re-Evaluation Project [6]. To facilitate the use of the tools under development with existing plant-specific data, they have a capability to generate flaw distributions based on files formatted by that tool in the same manner as is done in FAVOR.

These flaw population characterization files contain a set of 1000 tables of data, each of which is a unique distribution of the flaw population. These distributions define the density of flaws of a given through-thickness dimension, and for each dimension bin also define the distribution of the aspect ratio of flaws

having that dimension. In a PFM analysis, the first 1000 RPV realizations use the first 1000 flaw distributions sequentially, after which a counter is reset, and the flaw distributions are re-used in sequence.

Three separate files are used to define distributions of embedded flaws in plates and welds, and surface breaking flaws (which can be in either plate or weld regions). The generated flaws can be oriented in either the axial or circumferential orientations. In plate regions, the embedded flaws have equal probabilities of having axial or circumferential orientations. In weld regions, embedded flaws are oriented to align with the weld orientation. Inner surface-breaking flaws are all assumed to be in the circumferential orientation because of the process of applying the cladding, while outer surface-breaking flaw orientations are determined in the same manner as described above for embedded flaws.

The information stored about each flaw consists of the following data, all stored as variables in RAVEN:

- `depth_inner`: The depth of the innermost point of the flaw (zero for surface-breaking flaws)
- `depth_outer`: The depth of the outermost point of the flaw
- `aspect_ratio`: The aspect ratio of the flaw
- `orientation`: Flag denoting whether the flaw is axially or circumferentially oriented

2.3 Chemistry Sampling

The content of the alloying elements Cu, Ni, Mn and P is sampled, and the sampled contents are used as input in the EONY embrittlement correlation. The sampling scheme follows that in FAVOR and is outlined in this section.

The user provides the following input:

- For each subregion: best estimates in weight% of the chemistry content: $\mathrm{Cu}_{\mathrm{subr}}$, $\mathrm{Ni}_{\mathrm{subr}}$, $\mathrm{Mn}_{\mathrm{subr}}$, $\mathrm{P}_{\mathrm{subr}}$
- Standard deviations of normal distributions for weld chemistry content: $\sigma_{\mathrm{Cu,RPV}}$, $\sigma_{\mathrm{Ni,RPV}}$, $\sigma_{\mathrm{Mn,RPV}}$, $\sigma_{\mathrm{P,RPV}}$
- Standard deviations of normal distributions for plate chemistry content: $\sigma_{\mathrm{Cu,RPV}}$, $\sigma_{\mathrm{Ni,RPV}}$, $\sigma_{\mathrm{Mn,RPV}}$, $\sigma_{\mathrm{P,RPV}}$

For each RPV realization, the global standard deviation of Mn in plates or forgings is sampled.

$$\widehat{\sigma}_{\mathrm{Mn,RPV}} \leftarrow \begin{cases} \mathrm{Weibull}(0, 0.06933, 2.4708) & \text{wt\% in plates} \\ \mathrm{JohnsonSB}(0.00163, 0.03681, 0.83358, 1.15153) & \text{wt\% in forgings} \end{cases}$$

For each subregion of the RPV realization, the global subregion chemistry content is sampled. For plate and forging subregions, the content is sampled from normal distributions defined by the best estimate means and standard deviations input by the user.

$$\begin{aligned} \widehat{\mathrm{Cu}}_{\mathrm{subr}} &\leftarrow \mathcal{N}(\mathrm{Cu}_{\mathrm{subr}}, \sigma_{\mathrm{Cu,RPV}}) \\ \widehat{\mathrm{Ni}}_{\mathrm{subr}} &\leftarrow \mathcal{N}(\mathrm{Ni}_{\mathrm{subr}}, \sigma_{\mathrm{Ni,RPV}}) \\ \widehat{\mathrm{Mn}}_{\mathrm{subr}} &\leftarrow \mathcal{N}(\mathrm{Mn}_{\mathrm{subr}}, \widehat{\sigma}_{\mathrm{Mn,RPV}}) \\ \widehat{\mathrm{P}}_{\mathrm{subr}} &\leftarrow \mathcal{N}(\mathrm{P}_{\mathrm{subr}}, \sigma_{\mathrm{P,RPV}}) \end{aligned}$$

For weld subregions, the standard deviations of the normal distributions for Cu, Ni and Mn are sampled from specific normal distributions. The subregion chemistry content is then sampled from normal distributions defined by the best estimate means and the sampled standard deviations.

$$\begin{aligned}
\widehat{\sigma}_{\mathrm{Cu}} &\leftarrow \mathcal{N}(0.167 \times \mathrm{Cu}_{\mathrm{subr}}, \min(0.0718 \times \mathrm{Cu}_{\mathrm{subr}}, 0.0185)) \\
\widehat{\sigma}_{\mathrm{Ni}} &\leftarrow \mathcal{N}(0.029, 0.0165) \\
\widehat{\sigma}_{\mathrm{Mn}} &\leftarrow \mathrm{Weibull}(0.01733, 0.04237, 1.83723)
\end{aligned}$$

$$\begin{aligned}
\widehat{\mathrm{Cu}}_{\mathrm{subr}} &\leftarrow \mathcal{N}(\mathrm{Cu}_{\mathrm{subr}}, \widehat{\sigma}_{\mathrm{Cu,subr}}) \\
\widehat{\mathrm{Ni}}_{\mathrm{subr}} &\leftarrow \mathcal{N}(\mathrm{Ni}_{\mathrm{subr}}, \widehat{\sigma}_{\mathrm{Ni,subr}}) \\
\widehat{\mathrm{Mn}}_{\mathrm{subr}} &\leftarrow \mathcal{N}(\mathrm{Mn}_{\mathrm{subr}}, \widehat{\sigma}_{\mathrm{Mn,subr}}) \\
\widehat{\mathrm{P}}_{\mathrm{subr}} &\leftarrow \mathcal{N}(\mathrm{P}_{\mathrm{subr}}, \widehat{\sigma}_{\mathrm{P,subr}})
\end{aligned}$$

For each flaw, the local chemistry is calculated as the sum of the global chemistry and a small local variability. Mn has a larger local variability and is sampled from a normal distribution.

$$\begin{aligned}
\widehat{\mathrm{Cu}}_{\mathrm{flaw}} &= \widehat{\mathrm{Cu}}_{\mathrm{subr}} + \widehat{\Delta}_{\mathrm{Cu}} \\
\widehat{\mathrm{Ni}}_{\mathrm{flaw}} &= \widehat{\mathrm{Ni}}_{\mathrm{subr}} + \widehat{\Delta}_{\mathrm{Ni}} \\
\widehat{\mathrm{Mn}}_{\mathrm{flaw}} &= \mathcal{N}(\widehat{\mathrm{Mn}}_{\mathrm{subr}}, \widehat{\sigma}_{\mathrm{Mn}}) \\
\widehat{\mathrm{P}}_{\mathrm{flaw}} &= \widehat{\mathrm{P}}_{\mathrm{subr}} + \widehat{\Delta}_{\mathrm{P}}
\end{aligned}$$

For plates, the local variability is calculated by:

$$\begin{aligned}
\widehat{\Delta}_{\mathrm{Cu}} &\leftarrow \mathrm{Logistic}(-3.89 \times 10^{-7}, 0.00191) \\
\widehat{\Delta}_{\mathrm{Ni}} &\leftarrow \mathrm{Logistic}(-1.39 \times 10^{-7}, 0.00678) \\
\widehat{\Delta}_{\mathrm{P}} &\leftarrow \mathrm{Logistic}(1.3 \times 10^{-5}, 0.000286) \\
\widehat{\sigma}_{\mathrm{Mn}} &\leftarrow \mathrm{JohnsonSB}(0.00163, 0.03681, 0.83358, 1.15153)
\end{aligned}$$

For welds, the local variability is calculated by:

$$\begin{aligned}
\widehat{\Delta}_{\mathrm{Cu}} &\leftarrow \mathrm{Logistic}(6.85 \times 10^{-8}, 0.0072) \\
\widehat{\Delta}_{\mathrm{Ni}} &\leftarrow \mathrm{Logistic}(-0.0014, 0.00647) \\
\widehat{\Delta}_{\mathrm{P}} &\leftarrow \mathrm{Logistic}(3.27 \times 10^{-6}, 0.000449) \\
\widehat{\sigma}_{\mathrm{Mn}} &\leftarrow \mathrm{JohnsonSB}(0.00163, 0.03681, 0.83358, 1.15153)
\end{aligned}$$

2.4 $\mathrm{RT_{NDT}}$ Sampling

The transition temperature $\mathrm{RT_{NDT}}$ characterizes the irradiation-induced embrittlement of the RPV steel. The shift in $\mathrm{RT_{NDT}}$, $\Delta\mathrm{RT_{NDT}}$, compared to the unirradiated value, $\mathrm{RT_{NDT(0)}}$, is estimated using the EONY model

based on the sampled chemistry content of the steel and the neutron fluence at the depth of the flaw [7]. $\mathrm{RT_{NDT}}$ for each flaw is calculated using the formula:

$$RT_{\mathrm{NDT}} = \widehat{RT}_{\mathrm{NDT(0)}} - \widehat{RT}_{\mathrm{epistemic}} + \widehat{\Delta RT}_{\mathrm{NDT}} \tag{2}$$

The epistemic uncertainty, $\mathrm{RT_{epistemic}}$ is included to account for the difference between values of $\mathrm{RT_{NDT}}$ and $\mathrm{T_0}$ estimated directly from fracture toughness data using the Master Curve method [3]. The magnitude of $\mathrm{RT_{epistemic}}$ is sampled once for each subregion of an RPV realization from a distribution given by:

$$\widehat{RT}_{\mathrm{epistemic}} = \mathrm{Weibull}(-29.5, 78.0, 1.73) \tag{3}$$

For each flaw, $\widehat{RT}_{\mathrm{NDT(0)}}$ is sampled from a normal distribution defined by the mean $\mathrm{RT_{NDT(0)}}$ and standard deviation $\sigma_{RT_{\mathrm{NDT(0)}}}$ of the subregion (input by the user).

$$\widehat{RT}_{\mathrm{NDT(0)}} = \mathcal{N}(RT_{\mathrm{NDT(0)}}, \sigma_{RT_{\mathrm{NDT(0)}}}) \tag{4}$$

2.5 Failure Computation

To compute the probability of failure of a flaw with given geometric and chemistry characteristics requires that the embrittlement be characterized, and then that the history of K_I be computed. Once these are available, the CPI can be computed using a temperature-dependent Weibull distribution. The embrittlement is currently computed using the EONY model [4], which is based on data obtained from surveillance specimens, and is valid for the range of irradiation exposure observed in the current nuclear reactor fleet.

In general, computation of the stress intensity factor for a flaw can be a computationally expensive process. It can be computed for a specific flaw geometry and loading condition using a detailed 3D finite element model. Because of the large number of flaws that must be evaluated, it is not practical to run such models for each flaw sample, so reduced order models (ROMs) to represent K_I as a function of flaw geometry and loading are employed. The ROMs used in the current work to compute stress intensity factors for surface-breaking and embedded flaws described in the following sections.

These are the same procedures used by the FAVOR code. There has also been work underway, as documented in [8], to evaluate a variety of surrogate modeling techniques to automatically generate ROMS for fracture mechanics models. This work has demonstrated promising results, and is planned to be applied to consider flaw geometries not represented by the current ROMS for axis-aligned flaws.

2.5.1 Surface-breaking Flaw K_I Calculation

Stress Intensity Factor Influence Coefficient Procedure The method used for deterministic analyses of circumferential or axial inner surface breaking elliptical flaws in the presence of cladding for mode I loading represents the combined effects of stresses in the base metal and cladding on K_I:

$$K_I = K_{I_{base}} + K_{I_{clad}} \tag{5}$$

where the stress intensity factor solution for a given flaw is found by calculating the stress intensity factors for the base material ($K_{I_{base}}$) and cladding ($K_{I_{clad}}$) individually. The individual K_I values are calculated using the principle of linear superposition discussed in [9].

The method for obtaining the stress intensity factor for the base material requires the complete RPV through-wall stress distribution described by a cubic polynomial as well as a set of coefficients called Stress Intensity Factor Influence Coefficients (SIFICs). These components are combined in the following equation and used to determine the stress intensity factor for the base metal:

$$K_{I_{base}} = \sum_{i=0}^{3} C_j K_j \sqrt{\pi a} \tag{6}$$

In Equation 6, a is the flaw depth, K_j are the SIFICs, and C_j are the coefficients to the polynomial used to describe the through-wall stress distribution in the base material. The function weights are obtained using a least squares polynomial fit, shown in Equation 7:

$$\sigma\left(\frac{a'}{a}\right) = C_0 + C_1\left(\frac{a'}{a}\right) + C_2\left(\frac{a'}{a}\right)^2 + C3\left(\frac{a'}{a}\right)^3 \tag{7}$$

The SIFICs for the base material used in equation 6 are obtained through finite element models for specific flaw geometries, and curve-fitting techniques can used to obtain these for other flaw geometries. Each SIFIC for the base metal is determined as a function of the RPV's wall thickness relative to its inner radius (R/t), the relative flaw depth (a/t) and the flaw aspect ratio (L/a). The appropriate SIFICs are determined based upon the provided RPV and flaw geometry using a library of previously determined solutions. After the stress polynomial coefficients and corresponding SIFICs have been determined, the base metal component of equation 6 can be determined using Equation 7.

It is important to recall that this analysis is for a transient process. Therefore the global RPV finite element model is subjected to boundary conditions that vary over time, and is evaluated at each time step specified in the sequence. This means that at each time step in the simulation, the stresses at each of the radial positions will change. The SIFICs, however, are constant through the transient simulation because they are a function only of geometry. Thus, the coefficients in equation 7 must be determined and stored for every time step in the simulation. Additionally, new coefficients must be determined for every flaw length that is considered in each deterministic analysis. This is shown by Equation 7, where a' is a radial distance spanning from zero to a, which is the depth of the flaw being evaluated in the deterministic analysis. Because the polynomial is fit over the length of the flaw being considered, the polynomial must be determined for each flaw that is analyzed. This process can be repeated for any flaw length, a, such that the value is contained within the domain of SIFIC data.

The SIFICs for the base metal are independent of cladding effects, and the contributions of base metal and cladding are linearly superimposed. The stress intensity factor for the cladding is determined through the application of the weighting function similar to the method described for the base metal calculation. The cladding function weights require the coefficients from two separate linear polynomials. The first is a linear least squares fit of the stresses in the cladding as a function of the corresponding radial positions. This polynomial is fit over the full thickness of the cladding material and is not related to crack depth. The resulting polynomial is described by two coefficients, which will be referred to as the actual coefficients. The second set of coefficients is obtained by extrapolating a line through the thickness of the cladding using the two inner-most stress values located within the base material. The final coefficients used as the function weights in equation 8 are obtained by subtracting the extrapolated coefficients from the actual coefficients.

$$K_{I_{clad}} = \sum_{i=0}^{1} C_j K_j \sqrt{\pi a} \tag{8}$$

Once the coefficients for the cladding have been determined, the appropriate SIFICs can be selected and used in Equation 8 to determine the stress intensity factor for the cladding. These values are parameterized using the same geometric characteristics used in the base metal SIFICs, in addition to a cladding thickness parameter. The appropriate values are determined using interpolation within a dataset of pre-determined finite element solutions provided in the FAVOR Theory and Implementation Manual. The final result can

then be determined using equation 5, where the base metal and cladding stress intensity factors are summed, resulting in the total stress intensity factor for the flaw of interest.

A3000 module Earlier versions of FAVOR computed the SIFICs using the procedure described above by interpolation between values obtained from finite element solutions of specific flaw geometries. A new procedure was implemented in FAVOR that uses closed form expressions for SIFICs as documented in section A3000 of the ASME Boiler and Pressure Vessel Code. ORNL developed a Python module that incorporates implementation of ASME A3000 curve fits for the stress-intensity-factor influence coefficients (SIFIC) internal finite and infinite flaws with axial and circumferential orientations for RPV base material. The latter module is a Python implementation of the FAVOR capability already included in FAVOR since v. 15.3 [10]. The latter module was originally implemented in the Fortran language. ORNL transmitted this code to INL for integration into Grizzly.

For finite-length surface breaking flaws, revised SIFIC(s) provide consistency in the normalized flaw depths used in the databases for nominal R_i/t values of 10 and 20. Specifically, in the tables for $R_i/t = 20$, SIFICs are now given for the second relative flaw depth at $a/t = 0.0184$ (see Table B37 [10]); the latter relative flaw depth at the second position in the tabulation for $R_i/t = 20$ now matches that for $R_i/t = 10$ at the second position (see Table B2 [10]). In the original SIFIC tables, the relative flaw-depth values of a/t for $R_i/t = 10$ and 20 differ only in the second normalized flaw depth position in the tabulations (see Tables B2 and B11 [10]). The foregoing change was made to simplify interpolation of applied K_I factors for those intermediate values of R_i/t between 10 and 20, and to correct an error found in previous versions of FAVOR.

For infinite axial and 360°continuous circumferential internal surface-breaking flaws, the entire database of SIFICs was regenerated using the same scheme employed for finite-length, semielliptical internal surface-breaking flaws (see Section 5.1.3.2 [10] for a detailed description of that methodology which explicitly models the clad layer); the revised SIFIC database is given in Tables B38-B41 [10]. This change from previous versions of FAVOR was made to address issues identified for very shallow flaws where the effects of the cladding layer play a more significant role than is the case with deeper flaws. The motivation for this change is due to the fact that the original SIFIC database for infinite axial and 360°continuous circumferential internal surface-breaking flaws was generated in the early 1980s using a technique (see Section 5.1.3.2 [10]) that did not explicitly account for the effects of cladding. The revised SIFIC database now includes cladding effects consistent with the technique used for finite-length flaws.

2.5.2 Embedded Flaw K_I Calculation

The method for calculating Mode I stress intensity factors for embedded flaws follows that in [11], as presented in the FAVOR Theory Manual. It is based on resolving the applied stress field through the wall into the linear superposition of approximate membrane and bending stress components. The membrane and bending stress components are obtained by fitting a straight line through the stresses at the two crack tips and recording the value at the midpoint through the wall and at the (outer or inner) surface, respectively.

$$\sigma_m = \hat{\sigma}(t/2) = \frac{\sigma(x_2) - \sigma(x_1)}{2a} \times (t/2 - x_1) + \sigma(x_1) \tag{9}$$

$$\sigma_b = \hat{\sigma}(0) - \sigma_m = \frac{\sigma(x_1) - \sigma(x_2)}{2a} \times (t/2) \tag{10}$$

The stress intensity factor, K_I, is computed as a linear superposition of the membrane and bending stress components using the relation:

$$K_I = (M_m \sigma_m + M_b \sigma_b)\sqrt{\pi a/Q}, \tag{11}$$

where

$$2a = \text{the minor axis of the elliptical subsurface flaw} \tag{12}$$
$$Q = \text{flaw shape parameter} \tag{13}$$
$$M_m = \text{free-surface correction factor for membrane stress} \tag{14}$$
$$M_b = \text{free-surface correction factor for bending stress} \tag{15}$$
$$\sigma_m = \text{membrane stress} \tag{16}$$
$$\sigma_b = \text{bending stress} \tag{17}$$

The shape factor, Q, is given by the complete elliptic integral of the second kind:

$$Q(x) = E^2(x) \tag{18}$$
$$E(x) = \int_0^{\pi/2} \sqrt{1 - x\sin^2\theta}\, d\theta \qquad \text{for } 0 \le x \le 1 \tag{19}$$
$$x = 1 - 4\left(\frac{a}{L}\right)^2 \tag{20}$$

The free-surface correction factors for membrane stress and bending stress are defined in equations 21 and 22, respectively. In these equations, a is half of the flaw length in the radial direction and e is the distance between the midpoint through the wall and the midpoint of the flaw.

$$M_m = D_1 + D_2(2a/t)^2 + D_3(2a/t)^4 + D_4(2a/t)^6 + D_5(2a/t)^8 + \frac{D_6(2a/t)^{20}}{\left[1 - (2e/t) - (2a/t)\right]^{1/2}} \tag{21}$$

where:

$D_1 = 1$
$D_2 = 0.5948$
$D_3 = 1.9502(e/a)^2 + 0.7816(e/a) + 0.4812$
$D_4 = 3.1913(e/a)^4 + 1.6206(e/a)^3 + 1.8806(e/a)^2 + 0.4207(e/a) + 0.3963$
$D_5 = 6.8410(e/a)^6 + 3.6902(e/a)^5 + 2.7301(e/a)^4 + 1.4472(e/a)^3 + 1.8104(e/a)^2 + 0.3199(e/a) + 0.3354$
$D_6 = 0.303$

$$M_b = E_1 + \frac{A}{\left[1 - (2e/t) - (2a/t)\right]^{1/2}} \tag{22}$$
$$A = E_2(2e/t) + E_3(2e/t)^2 + E_4(2e/t)(2a/t) + E_5(2a/t)(2e/t)^2 + E_6(2a/t) + E_7(2a/t)^2 + E_8(2e/t)(2a/t)^2 + E_9$$

where:

$E_1 = 0.8408685$ $E_2 = 1.509002$ $E_3 = -0.603778$
$E_4 = -0.7731469$ $E_5 = 0.1294097$ $E_6 = 0.8841685$
$E_7 = -0.07410377$ $E_8 = 0.04428577$ $E_9 = -0.8338377$

3 Benchmarking

As the capabilities described in this report have been developed, individual components of the algorithm have been benchmarked against solutions from the FAVOR code. The results of the benchmarking efforts taken to-date are described here. This is only an initial effort, and a more thorough effort is planned for the coming fiscal year.

3.1 Individual Flaw CPI Calculations

A detailed set of outputs was generated from FAVOR to facilitate benchmarking of the CPI calculation in Grizzly. These were provided by the FAVOR developers in a file containing the values of the sampled chemistry and embrittlement parameters for each flaw in a simple analysis of one surface-breaking flaw geometry per RPV realization. By eliminating random sampling from the Grizzly PFM analysis, the implementations of the RT_{NDT} and CPI calculations could be verified. Figure 3 shows a histogram of the the relative difference in CPI, which indicates very minor differences.

3.2 Flaw Sampling

Flaw sampling in Grizzly was benchmarked against FAVOR using a model of the cylindrical RPV beltline region with a 0.25 in thick clad on the inner surface. The beltline was treated as one plate subregion. Flaws in plates are typically located in a small region close to the inner surface; in order to generate a large number of flaws and get better statistics, a flaw characterization file for welds was used.

The number of flaws is deterministic, given the same flaw characterization file and RPV geometry, and were therefore identical in Grizzly and FAVOR for this analysis. Distributions of the depth of the innermost

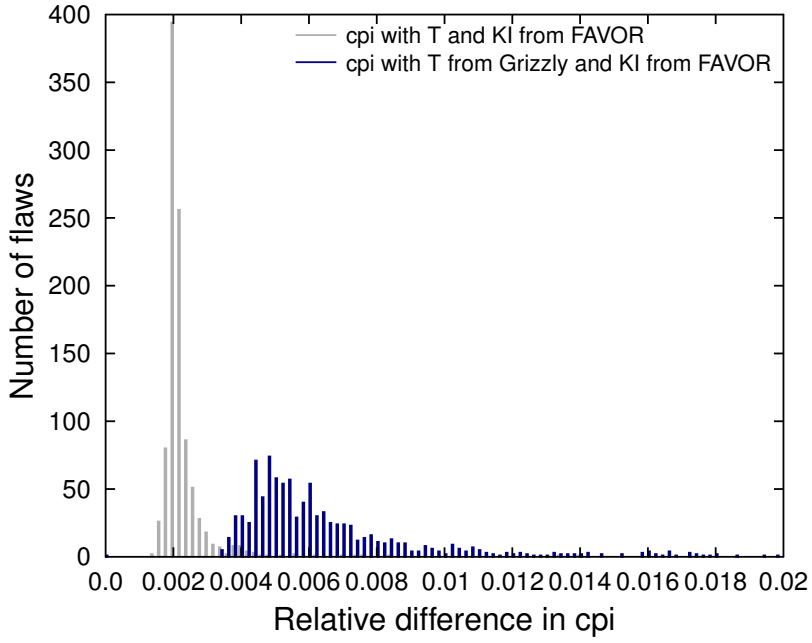

Figure 3: Difference in CPI between FAVOR and Grizzly in a deterministic analysis.

edge of the flaw, flaw size in the radial direction, and flaw aspect ratio are compared in Figure 4, and show close agreement between the codes.

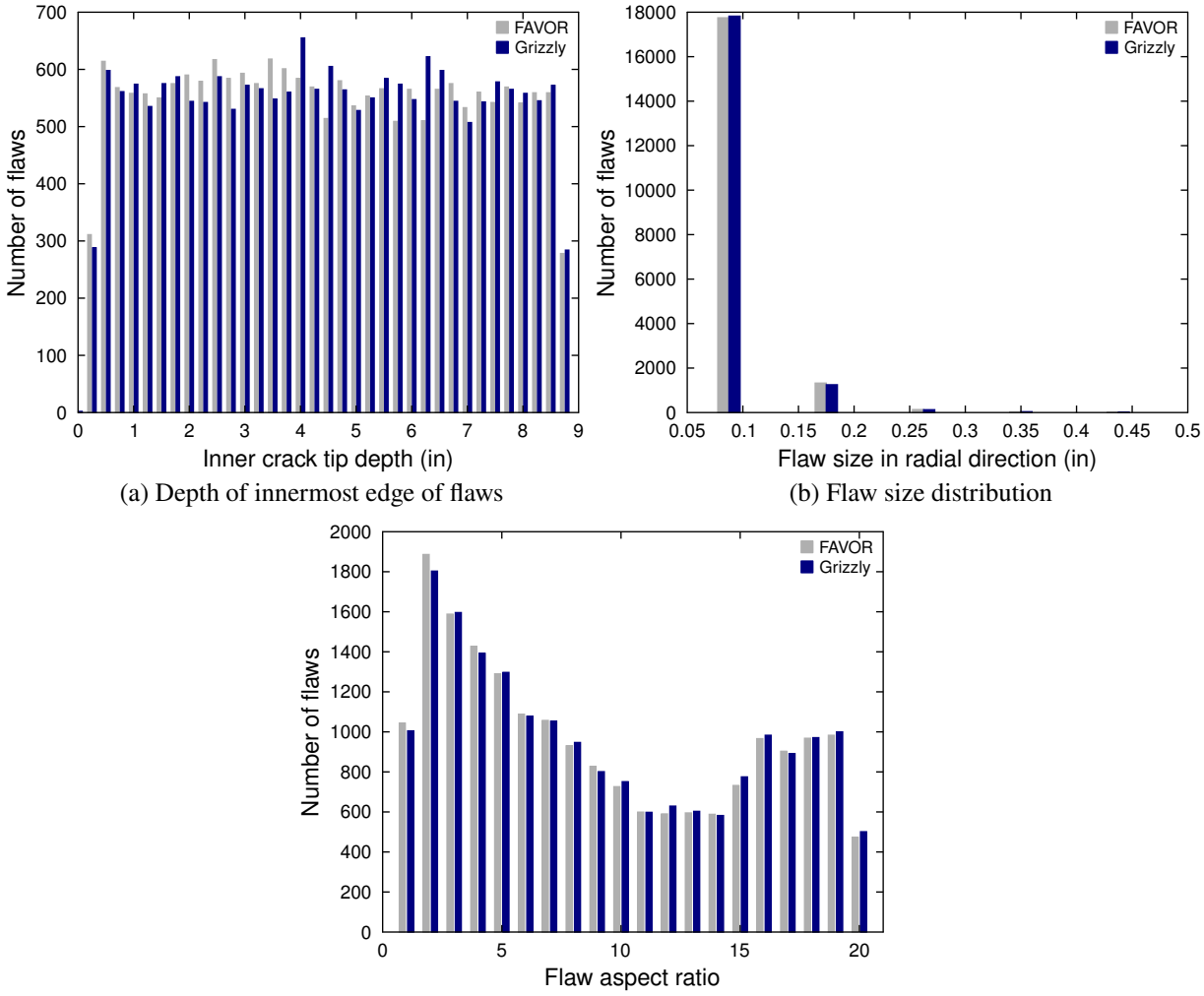

(a) Depth of innermost edge of flaws

(b) Flaw size distribution

(c) Flaw aspect ratio distribution

Figure 4: Distributions of flaw characteristics in an RPV realization in Grizzly and FAVOR. The total number of flaws was 19259 in both Grizzly and FAVOR.

3.3 Overall CPI Calculations

A complete thermomechanical loading and PFM analysis was performed in Grizzly and compared with the same analysis in FAVOR. Temperature and stress fields in the RPV wall during a severe PTS transient were obtained in a deterministic thermomechanical analysis in Grizzly. The temperature and pressure history of the transient is shown in Fig. 5 and the mesh representation of the RPV beltline is shown in Fig. 6. For simplicity, this analysis did not include cladding. During the analysis, third order polynomials were fit automatically using MOOSE postprocessors to the one-dimensional temperature and stress profiles through the wall at each timestep.

The fit functions were subsequently used in the PFM part of the calculation to look up temperature and stress at the depth of the flaw. The probabilistic analysis was confined to a 5 inches tall and 120 degree wide

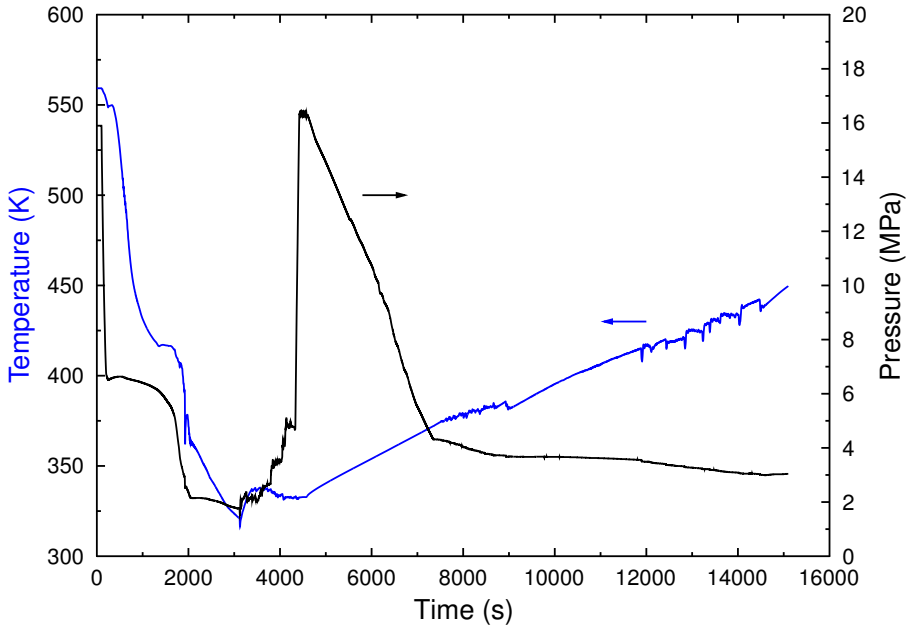

Figure 5: Time histories of coolant temperature and pressure applied as boundary conditions to 2D strip model of RPV beltline region.

section of the beltline region. The average number of flaws in this region over 1000 RPV realizations was 111.6. In Grizzly, 2.4% of flaws had a CPI larger than zero, while for FAVOR that number was 2.2%. The average CPI over the 1000 RPV realizations was 0.01835 in FAVOR and 0.00134 in Grizzly.

The sources of this discrepancy in the results are still under investigation. Many of the components of the analysis have been checked and compare well with FAVOR, but there are still more components of the algorithm that need to be checked individually against FAVOR to ensure that they are in agreement.

The distributions of RT_{NDT} from Grizzly and FAVOR for flaws in 100 RPV realizations are compared in Fig. 7. The results generally agree well, except for the tails of the distributions at very low transition temperatures. The difference may be due to subtle differences in the sampling procedures and needs to be investigated further.

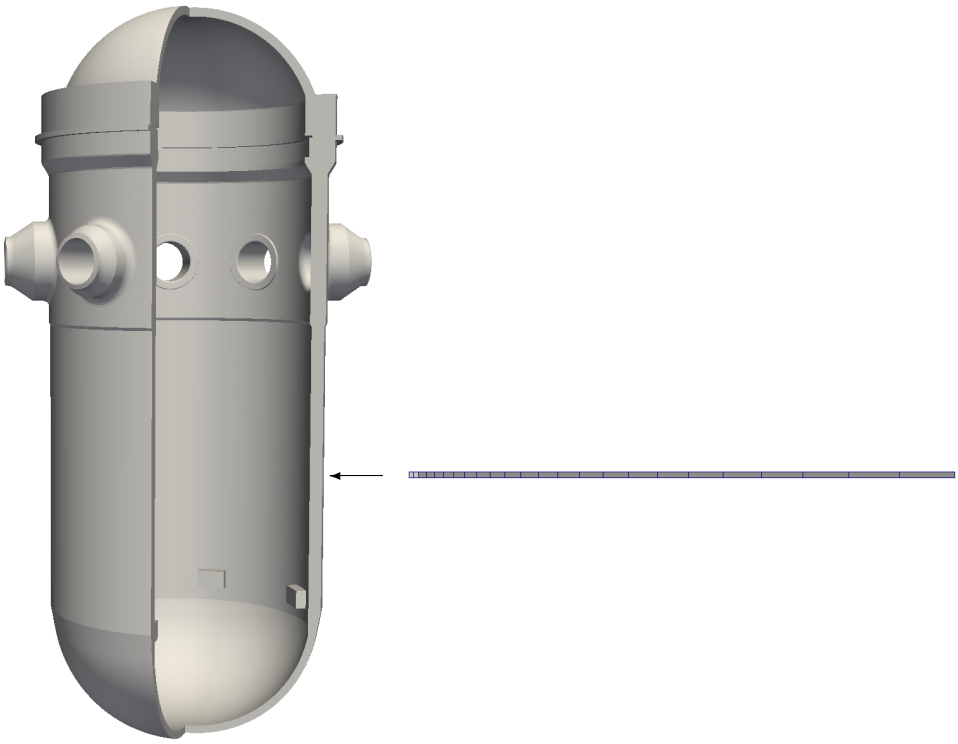

Figure 6: Cutaway of representative RPV (left), and finite element mesh (right) used to represent the beltline region using a 2D strip model. The inner radius of the wall is 86 in and the wall thickness is 8.75 in.

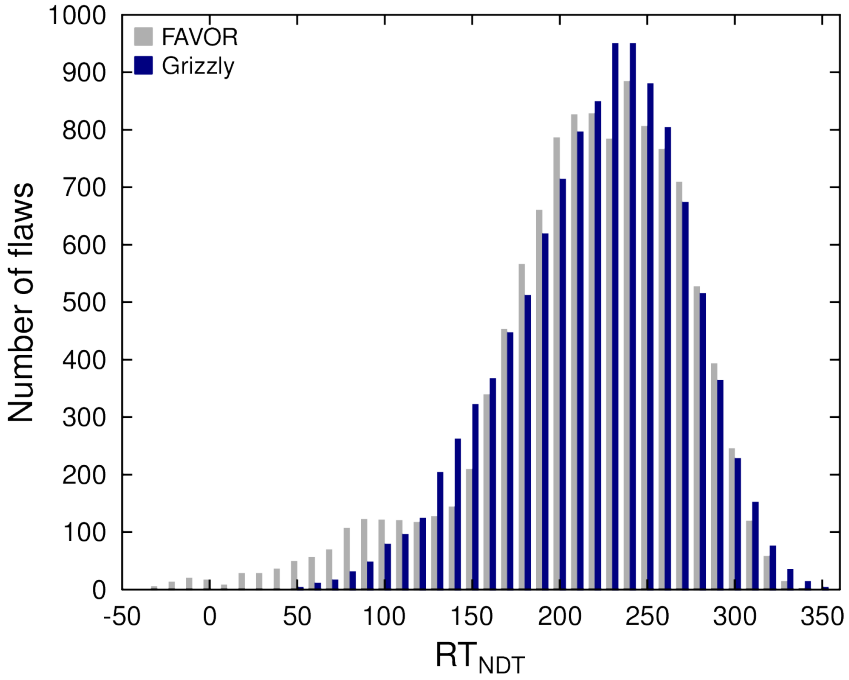

Figure 7: Comparison of RT_{NDT} distributions in the same plate analysis in Grizzly and FAVOR.

4 Summary and Future Development

4.1 Summary of Current Developments

This report documents work to develop and perform initial testing of a capability to perform PFM analyses of an RPV containing a population of flaws. The following code developments were made in support of this work:

- A specialized sampling module that mimics the two-level sampling strategy used by FAVOR was developed.
- A capability to generate populations of flaws based on probabilistic descriptions of flaw geometry from the VFLAW code was developed.
- A capability to generate samples of RPV steel chemistry parameters was developed.
- Code modules to use ROMs to compute K_I for embedded and surface-breaking flaws were developed.
- Initial benchmarking of these newly developed code modules against FAVOR solutions was performed.

4.2 Planned future work

The following developments are planned to develop a complete PFM capability:

- More thorough benchmarking of individual components and the capability in its entirety will be performed against the FAVOR code, and issues will be resolved.
- Missing capabilities currently available in FAVOR will be implemented. These include the following:
  - An ability to compute CPF in addition to CPI
  - An ability to evaluate multiple transients
- The entire capability documented here will be made available in the Grizzly code base after an API is developed for `Sampler` classes in RAVEN.
- An ability to integrate higher-dimensionality models for the global response of RPVs with these PFM algorithms will be developed.
- An ability to use ROMs to rapidly compute fracture parameters for flaw geometries that cannot currently be evaluated will be developed.

4.3 Benefits of this approach

When complete, the RAVEN/Grizzly approach being developed will provide the following benefits for probabilistic fracture analysis of RPVs under transient conditions:

- Grizzly and RAVEN are both built on modern, flexible code infrastructures that provide many basic facilities that are leveraged for this specific application.
- RAVEN provides advanced techniques that can greatly speed up the process of probabilistic fracture analysis, including adaptive sampling techniques and parallel processing.

- The 2D and 3D capabilities provided by Grizzly can be used to represent local nonuniformities in the global reactor pressure vessel response, such as local geometric effects and effects introduced by a nonuniform thermal environment.
- The reduced order model capability being developed in Grizzly will permit automated generation of models that can be rapidly evaluated for a wide variety of flaw configurations.

5 References

1. B. Spencer, M. Backman, P. Chakraborty, and W. Hoffman, *Reactor Pressure Vessel Fracture Analysis Capabilities in Grizzly*, INL/EXT-15-34736, Idaho National Laboratory, Idaho Falls, ID, Mar. 2015.
2. T. Dickson, P. T. Williams, and S. Yin, *Fracture Analysis of Vessels – Oak Ridge, FAVOR, v12.1, Computer Code: User's Guide*, ORNL/TM-2012/566, USNRC Adams number ML13008A016, Oak Ridge National Laboratory, Oak Ridge, TN, Nov. 2012.
3. P. Williams, T. Dickson, and S. Yin, *Fracture Analysis of Vessels – Oak Ridge, FAVOR, v12.1, Computer Code: Theory and Implementation of Algorithms, Methods, and Correlations*, ORNL/TM-2012/567, USNRC Adams number ML13008A015, Oak Ridge National Laboratory, Oak Ridge, TN, Nov. 2012.
4. E. Eason, G. Odette, R. Nanstad, and T. Yamamoto, "A physically-based correlation of irradiation-induced transition temperature shifts for RPV steels", *Journal of Nuclear Materials*, vol. 433, no. 1-3, pp. 240–254, Feb. 2013.
5. B. Spencer, W. Hoffman, S. Sen, C. Rabiti, T. Dickson, and R. Bass, *Initial Probabilistic Evaluation of Reactor Pressure Vessel Fracture with Grizzly and RAVEN*, INL/EXT-15-37121, Idaho National Laboratory, Idaho Falls, ID, Oct. 2015.
6. F. A. Simonen, S. R. Doctor, G. J. Schuster, and P. G. Heasler, *A Generalized Procedure for Generating Flaw-Related Inputs for the FAVOR code*, NUREG/CR-6817, PNNL-14268, Pacific Northwest National Laboratory, Richland, WA, Mar. 2004.
7. B. Spencer, J. Busby, R. Martineau, and B. Wirth, *A Proof of Concept: Grizzly, the LWRS Program Materials Aging and Degradation Pathway Main Simulation Tool*, Idaho National Laboratory, Idaho Falls, ID, 2012.
8. W. M. Hoffman, M. E. Riley, and B. W. Spencer, "Surrogate Model Development and Validation for Reliability Analysis of Reactor Pressure Vessels", *ASME Pressure Vessels and Piping Conference*, PVP2016-63341, Vancouver, BC, Canada, July 2016.
9. H. F. Bückner, "A Novel Principle for the Computation of Stress Intensity Factors", *Z. angew. Math. Mech.* Vol. 50, pp. 529–546, 1970.
10. P. Williams, T. L. Dickson, S. Yin, and B. R. Bass, *Fracture Analysis of Vessels – Oak Ridge, FAVOR, v15.3, Computer Code: Theory and Implementation of Algorithms, Methods, and Correlations*, ORNL/LTR-2016/71, ORNL/TM-2016/61454, Oak Ridge National Laboratory, Oak Ridge, TN, 2015.
11. R. C. Cipolla, *Computational Method to Perform the Flaw Evaluation Procedure as Specified in the ASME Code, Section XI, Appendix A*, EPRI Report NP-1181, Failure Analysis Associates, Sept. 1979.